Soft Matter

Anisotropic Phase-Separated Morphology of Polymer Blends Directed by Electrically Pre-oriented Clay Platelets

Journal:	*Soft Matter*
Manuscript ID	SM-ART-12-2019-002379.R1
Article Type:	Paper
Date Submitted by the Author:	12-Jan-2020
Complete List of Authors:	Yook, Sungho; Purdue University Isik, Tugba; Purdue University, Materials Engineering Ortalan, Volkan; University of Connecticut, Materials Science and Engineering Cakmak, Mukerrem; Purdue. University, Materials and Mechanical Engineering Departments

ARTICLE

Anisotropic Phase-Separated Morphology of Polymer Blends Directed by Electrically Pre-oriented Clay Platelets

Received 00th January 20xx,
Accepted 00th January 20xx

DOI: 10.1039/x0xx00000x

Sungho Yook,[a] Tugba Isik,[bc] Volkan Ortalan[cd] and Mukerrem Cakmak*[a]

We describe a general pathway to prepare an anisotropic phase-separated polystyrene (PS) - poly(vinyl methyl ether) (PVME) blend morphology by using electrically pre-orientated clay platelets. The clay platelets were oriented in a PS/PVME blend by means of an externally applied AC electric field while the blend is in one phase. Following orientation step, phase separation of the blends was induced by a temperature jump above their lower critical solution temperature (LCST) in the presence of the oriented clay platelets. In this process, an early stage co-continuous PS / PVME morphology coarsened and turned anisotropic phase-separated morphology parallel to the direction defined by clay planes oriented by AC electric field. The degree of anisotropy of PS / PVME phase-separated morphology was characterized by image analysis and that was found to be linearly proportional to the degree of orientation of clay platelets obtained by a 2D Wide Angle X-ray Scattering (WAXS). Transmission Electron Microscope (TEM) image of the blend morphology revealed that clay platelets oriented to AC field direction were located in a PVME phase. The electrically ordered column structures of clay platelets in the PVME phase yielded anisotropic PS diffusion during the phase separation. This process provides a unique new way to develop directionally organized phase-separated morphology from partially miscible binary blends using nanoparticles in combination with an external electric field.

1. Introduction

The control of the morphology in a polymer blend is essential as the properties of the polymer blends are highly dependent on their morphology.[1,2] The development of the desired nano/micro structure in block copolymers, partially miscible polymer blends, and immiscible homopolymers have been widely demonstrated. Among different types of morphologies, the globally well-oriented morphologies are an ideal structural motif particularly for enhancing desired functional properties such as proton conductivity in a proton-exchange membrane[3] or efficiency in an organic photovoltaic cell[4] in the desired direction. However, the directionally oriented morphology in immiscible polymer blends is difficult to achieve because the phase separation generally occurs isotopically in the absence of external forces.

To produce oriented morphology in polymer blends, shear[5,6] / electric[7–10] / magnetic[11] forces can be applied. The use of shear field during phase separation usually lead to formation of string-like phase-separated morphology with the primary axes oriented along the flow direction. This deformation of polymer fluids is due to the softening of interfacial tension between two fluids at high shear rate. Beside shear fields, external electric-field can be used to produce anisotropic structures. When an electric field is applied to binary fluids, electric stresses are produced at fluid-fluid boundaries due to the difference in electrical properties of two fluids.[12,13] The shape of binary morphology in the electric field is determined by the balance between electric stress and interface tensions of two polymeric fluids.

Krause et al. showed the anisotropically phase-separated morphology of two immiscible polymers under the electric field during phase separation induced by a solvent removal.[7–9] They found the columnar structures of PMMA domains in a PS domain while a common solvent of two polymers (toluene) was evaporated. Despite anisotropic phase-separated morphology, the final morphology in this study was not only influenced by the electric field but also by solution drying kinetics. During polymer solution drying, the rapid solvent evaporation from the top surface of the film generates inhomogeneity in solvent concentration in the film. Furthermore, the solvent generally prefers one of the components in the blends. These two effects can lead to nonuniform component distribution along the film thickness direction during drying.[14,15] Thermally induced phase separation of partially miscible polymer blends is a better alternative method to avoid the problem caused by solvent drying.

Urakawa et el. examined the morphology of a partially miscible polymer blend near critical temperature under the electric field.[10] They observed anisotropic phase-separated Poly(2-chlorostyrene) (P2CS) and poly(vinyl methyl ether) (PVME) morphologies when lithium perchlorate ($LiClO_4$) were dissolved in the blend. The role of $LiClO_4$ in the blends was to enhance the difference of electrical properties in two polymer phases. They reported that P2CS and PVME domains were oriented parallel to the electric field direction in the process of phase separation.

[a]*School of Materials Engineering, Purdue University, West Lafayette, Indiana 47907, USA E-mail: cakmak@purdue.edu*
[b]*School of Mechanical Engineering, Purdue University, West Lafayette, Indiana 47907, United States*
[c]*Institute of Materials Science, University of Connecticut, Storrs, Connecticut 06269, United States*
[d]*Materials Science and Engineering, University of Connecticut, Storrs, Connecticut 06269, United States*
† Electronic Supplementary Information (ESI) available: See DOI: 10.1039/x0xx00000x

Adding compatibilizers in polymer blends is another way to control the morphology in polymer blend. Surface-tailored nanoparticles,[16–20] block copolymers,[21–23] and organically-modified clay platelets[24–29] in a binary blend have been considered as effective compatibilizers. It has been reported that the compatibilizers stabilized the morphologies of immiscible blends by reducing interfacial tension via interfacial localization or increasing viscosity of the blends.[27] Moreover, some colloidal particles even freeze the nonequilibrium co-continuous structure of blend morphology by aggregating at the interface and ultimately lead to a stable co-continuous morphology called a "bijel".[18–20,30–32] Although the morphology of the blends can be stabilized by adding compatibilizers, the anisotropic morphology is still hard to achieve due to intrinsically isotropic demixing of polymer blends.

From this viewpoint, the presence of well-oriented particles in polymer blends may influence the phase separation mechanism by directionally affecting the diffusion process by their presence. If they are organized to create large barriers, the effect of particles on the phase-separated morphology would be further amplified. Organically-modified clay platelets are good candidates for forming particle barriers as they exhibit 2D platelet shapes. They are also easily aligned in the AC electric field due to high polarizabiliy[33–35] on the surface of particles. Therefore, we hypothesize that the clay platelets, having large 2D surface area and high polarization under electric fields, can be applied to develop anisotropic morphology in blends.

In the current study, we report a novel approach to produce anisotropic phase-separated morphology in a bulk polystyrene (PS) - poly(vinyl methyl ether) (PVME) blend near critical temperature as directed by pre-oriented clay platelets in AC field. The evolution of morphology at near critical composition from co-continuous structure to coarsened anisotropic structure was investigated with microscopes and X-ray scattering techniques at different annealing time and electric field strength.

2. Experimental Section

2.1 Materials

PS (Mw: 35kg/mol) was purchased by Sigma Aldrich and used as received. PVME (Mw: 30kg/mol) was purchased from Polysciences Inc. as 50 % aqueous solution. The residual water in PVME material was removed by drying the solution overnight at 120°C in vacuum oven before usage. The organically-modified montmorillonite clay (Cloisite 15A) was provided by BYK Additives & Instruments.

2.2 Phase diagram

PS and PVME at a series of blend ratios were dissolved in toluene and casted on a cover glass at room temperature. The samples were dried overnight at 110°C in a vacuum oven to remove residual toluene solvent. Cloud points of the blends were determined by optical microscope (OM) observation on the heating stage. The temperature of the heating stage was stepwise increased 1°C every 5min until phase separation was observed under OM.

2.3 Sample Preparation

PS and PVME (50 / 50) homopolymers were dissolved in toluene by a planetary centrifugal mixer (Thinky Mixer) for 1 hour. After achieving a homogeneous polymer solution, the 5 vol % of clay platelets (respect to polymer) were dispersed in the polymer solution by Thinky Mixer for 3 hours. The sample was cast on a glass side between two copper electrodes (100 µm thickness and 50 mm length) with a 4 mm gap to create films with 40 µm ~ 60 µm final thickness. The AC electric field was applied to the sample with the initial viscosity of 0.98 Pa·s (ESI,† Fig. S1). The AC fields range of from 0 V/mm to 1000 V/ mm with 100 Hz was generated by a high voltage amplifier (Matsusada, AMT-20B10-LC) and a function generator (HP, 33120A). During the application of the AC fields to the samples, toluene was gradually evaporated at room temperature. The electrically-oriented clay fillers in blends were immobilized as the sample were solidified. To remove residual toluene completely, the samples were dried in a vacuum oven at room temperature for a week. The PS / PVME phase-separation was induced for the samples on a 128°C hot plate (4°C above critical temperature) with N_2 gas purging in the presence of AC fields. The samples were annealed for different time from 5 mins to 120 mins. The identical AC field strength was applied for both drying and annealing process. The control samples without E-field were prepared under the same conditions. Overall sample preparation steps are shown in Fig 1. We mainly investigated a PS / PVME (50:50) blend with 5 vol% clay platelets throughout the study.

2.4 Morphological Analysis

The phase-separated morphology of PS / PVME blends was examined by OM (Leitz Laborlux 12 Pol S) (top view) and by Scanning Electron Microscope (Hitachi S-4800 Field Emission SEM) (cross-sectional view). The direction of imaging morphology and the corresponding direction of the application of the AC electric field were shown in Fig 1c. To observe cross-sectional morphology, the sample with ~50 thickness was fractured in liquid nitrogen. The PVME phase on cross-sectional plane was selectively extracted by immersing the sample in the methanol overnight. The remaining PS morphology was visualized by SEM after the samples were sputter-coated with 9 nm of Au/Pd. An accelerating voltage of 3 kV with 8 mm a working distance was used for SEM characterization. For WAXS experiments (Anton Paar SAXSpoint 2.0), X-ray beam with monochromatized to Cu Kα radiation was used. The X-ray beam orthogonal to the applied AC electric field (Fig 1c. Top View direction) was exposed to the samples. The sample to detector distance was 363 mm and X-ray exposure time was 5 minutes for each sample. The azimuthal plots of X-ray scattering pattern were constructed by integrating the scattering intensity from $q = 0.7\ nm^{-1}$ to $q = 2\ nm^{-1}$ for every 1° by using SAXS analysis software offered by Anton Paar. For the sample of TEM experiment, the cross-sectional samples were prepared by using a cryo-microtome (Leica UCT ultramicrotome with EMFCS cryo attachment). Ultrathin sections between 100 nm to 150 nm were cut on a diamond knife at -60 °C at a speed of 1.0 mm/s and collected on 100 mesh formvar/carbon coated double folding grids. TEM images were obtained using a FEI Talos 200 S/TEM transmission electron microscope operated at an accelerating voltage of 200 kV.

2.5 Image analysis

The characteristic domains size (ξ) of continuous PS and PVME domains was determined by the image analysis software (ImageJ). The OM images were transformed to black and white binary images

by highlighting the interface between two polymers. The interfacial length (L) was calculated by addling the length of interfacial lines. We defined the characteristic domains size (ξ) as total areas (A) over interfacial length (L) (ξ = A/L).[30] The detailed calculation was described in ESI,† Fig. S2.

3. Results and Discussion

The phase diagram of PS/PVME blend used in this study was shown in Fig. 2. The blend shows a typical LCST system, where the critical temperature of the blend is 124°C at 50/50 concentration. Since the presence of particles and/or AC electric fields may affect the critical temperature of the blend, we reviewed the relevant previous reports about the effect of nanoparticles and/or electric fields on the phase diagram. It was reported that the addition of 4 vol % layered silicate in PS/PVME blend does not affect the phase diagram.[29] However, high electric field may shift the phase separation temperature in a partially miscible polymer blend. Kriisa and Roth showed that the shift in phase separation temperature ($\Delta Ts(E) = Ts(E) - Ts(0)$) is proportional to the square of the applied electric field E^2.[36,37] They found that the shift in the critical temperature of a PS/PVME blend is followed by $\Delta Ts/E^2 = (4.8 \pm 0.4) \times 10^{-14}$ Km^2/V^2.[36] Based on this equation, the maximum electric field in this study (1MV/m) shows ΔTs is about 0.048K. Therefore, we consider that the presence of 5 vol% platelets or the application of the electric field less than 1kV/mm would not significantly alter the critical temperature in our experimental system. Prior to investigating the effect of clay fillers, a phase-separated morphology of a neat PS / PVME (50/50) blend was examined without the AC electric field to understand the emerging morphology near critical composition. When a partially miscible polymer blend undergoes spinodal decomposition by crossing phase boundary of the phase diagram at near-critical compositions, isotropic composition fluctuations appear with characteristic length (λ). These isotropic composition fluctuations yield a co-continuous structure at the early phase separation stage and the disordered co-continuous two-phase structure grows exponentially with time.[1,38] The neat PS / PVME (50/50) blend clearly exhibited co-continuous structure in the early stage as shown in Fig. 3. Due to difference in refractive index of each polymer (n_{PS} : 1.592, n_{PVME} :1.467), top view images of co-continuous morphology was characterized under OM (Fig. 3a – Fig. 3c). The corresponding cross-sectional SEM images of the films also visualized PS domains after selectively etching PVME phase (Fig. 3d- Fig. 3f). The isotropic co-continuous structure was coarsened with increasing characteristic domain sizes (ξ) over the annealing time as indicated by OM and SEM images. The isotropic composition fluctuations during the spinodal decomposition result in an isotropic phase-separated morphology.

To evaluate the effect of clay platelets in blends, we investigated the phase-separated morphology with non-oriented clay platelets with increasing annealing time. The cross-sectional morphologies over time were shown in Fig. 4. Although clay platelets were hard to distinguish with SEM, PS domains and etched domains (PVME domains) were clearly distinguishable after selectively dissolving PVME phase. Fig. 4b and Fig. 4c show that the isotropic 3D co-continuous structure appeared at the early stage of a phase separation. The disordered co-continuous structure was coarsened isotopically over annealing time with increasing characteristic domain sizes (ξ) even though the rate of phase-separation slowed down in the presence of 5 vol% of clay platelets.

With the electrically pre-oriented clay platelets (500V/mm, 100Hz), the evolution of morphology with time was observed to be quite different. The isotropic 3D co-continuous structure also appeared after 5 min annealing similar to the morphology with non-oriented clay platelets (Fig. 5a and Fig. 5b). However, the morphology coarsened and oriented over by growth of PS domains along the AC electric field direction as the phase separation progressed (Fig. 5c – Fig. 5f). Fig. 5f clearly shows that PS domains were elongated parallel to the AC field direction. In order to verify that the orientation of polymer domains is not due to the difference in electrical properties between two polymers, we also examined the phase-separated morphology under the AC field without clay platelets. The PS/PVME blend was isotopically coarsened in the presence of AC electric field (500V/mm, 100Hz) as shown in ESI,† Fig. S3. This result is attributed primarily to the small difference in electrical properties (i.e. dielectric constant and conductivity) between PS and PVME. The difference in dielectric constant of PS (ε~2.5)[39] and PVME (ε~4.0)[40] is small. The ionic conductivity of these materials also are negligible (PVME is around 10^{-10} -10^{-11} S/cm[41] and PS is around 10^{-12}-10^{-13} S/cm[39]). This small contrast in electrical properties may not create enough electrical and hydrodynamic stresses between two polymers at the AC electric field strength we used in this study (up to 1000V/mm). We also found that the degree of anisotropy in a phase-separated morphology was influenced by the concentration of the clay platelets (ESI,† Fig. S4). 1 vol% of clay platelets (500V/mm, 100Hz) in the blend developed an almost isotropic phase-separation morphology. As the concentration of clays increased to 2 vol%, a slight anisotropic morphology appeared as evidenced by 2D-FFT pattern shown in the inset of each optical microscopy image. High anisotropy of phase-separated morphology was found in the blend with 5 vol%. This result indicates that at least about 5 vol% of clay platelet loading needed to develop highly anisotropic phase-separated morphology.

It is also worth noting that the presence of 5 vol % clay platelets in a blend significantly slowed down the rate of phase separation (Fig. 6). The characteristic domain size (ξ) with annealing time can be characterized by the power law equation, $\xi(t) \propto t^{\alpha}$, where α is an exponent indicating the rate of phase separation.[10,42] All data points of the neat blend sample were fitted well by a power-law model with the high exponent (α = 2). However, the data points of the sample containing 5 vol % clay cannot be fitted by the power-law model as the last two data points showed a plateau. The result indicates that there was a significant suppression of phase coarsening by 5 vol % clay platelets in the last stage of phase separation in either presence or absence of AC field.

Anisotropic phase-separated morphology with oriented clay platelets more clearly appeared at the late stage of phase separation. Top view OM images and cross-sectional SEM images showed the morphology with and without AC field after 30 mins of annealing at 128°C (Fig. 7). The oriented and coarsened morphology clearly appeared in the sample containing 5 vol% oriented clay platelets (Fig. 7a and 7c). The PS phases (Dark regions) in OM image shows that PS domains with tens of micrometer size were elongated in the AC electric field direction in a PVEM phase. The corresponding

elongated PS phases were also identified in SEM image (dark regions). On the other hand, the sample containing 5 vol% non-oriented clay platelets exhibited isotropic phase-separated morphology. The PS phases in both OM and SEM images show that they were coarsened isotopically with annealing time with tens of micrometer size (Fig. 7b and 7d). Both sample also shows that the initial co-continuous PS/PVME morphology developed into large PS discrete domains in a continuous PVME phase in late stage of phase separation. Fast Fourier Transformation (2D-FFT) of images shown in the inset of each image indicates the degree of average anisotropy of Fig. 7a and 7b.

The effect of the AC electric field strength on the orientation of phase-separated domains was also examined. 5 vol % clay platelets were pre-oriented with the various strength of AC field in PS / PVME blends during drying process and then samples were annealed at 128°C for 60 min with corresponding electric field strength. Fig. 8 shows that the orientation of polymer domains depends on the strength of the AC electric fields. The isotropic PS domains with the size of several tens of micrometer were observed in a continuous PVME domain at 50 V/mm of AC field strength. As the field strength increased to 100 V/mm, the PS domains were slightly oriented to the AC field. Then, they were highly oriented to AC field direction above 500 V/mm. To numerically quantify the orientation degree of phase-separated morphology, we calculated the orientation order parameter (S) based on 2D-FFT patterns of each OM image. Accordingly, the integrated intensity of the 2D-FFT pattern was plotted against the azimuthal angle (ϕ). The integrated intensity of anisotropic 2D-FFT pattern showed a graph with two peaks at ϕ = 90° and 270°, whereas that of isotropic 2D-FFT pattern showed no significant peaks (ESI,† Fig. S5). By fitting the plots by a Maier-Saupe distribution function, we can obtain the orientation order parameter, which varies from 0 (totally random) to 1 (perfectly oriented). Fig. 8f shows the domain orientation order parameters as a function of the electric field strength. The graph shows that the orientation of domains was slightly increased to ~0.1 at 100 V/mm electric field intensity. When the field strength increased to 200 V/mm, the orientation parameter significantly increased to 0.6. A further increase in AC field strength to 500 V/mm caused a more increase of the orientation order parameter (up to ~0.8) and then leveled off with further increase of voltage.

In the presence of an electric field, the clay platelets undergo polarization. Due to shape anisotropy of clays, the polarization moment (μ) of clay platelets can be divided into two elements: one parallel to long axis ($\mu_{\parallel}$) and one perpendicular to long axis ($\mu^{\perp}$).[43,44] For clay platelets, the polarizability in the direction of the long axis is much larger than that in the perpendicular direction. This non-zero net polarization moment on the clays, which is not coordinated with the direction of the electric field, lead to field-induced torque (T) on clay platelets. The torques cause rotational and translational movement of clay platelets to the direction of the electric fields against the viscous drag force of the surrounding polymer medium.[34] Apart from this field-induced torque, the coulombic attraction is generated between oppositely charged particles.[44] The combined effects lead to the orientation of clay platelets and organization along columns in the electric fields.[33] In this study, the clay platelets were oriented in the AC electric fields during drying and the orientation was maintained during annealing process. To characterize the clay orientation in blends for each processing steps, 2D WAXS analysis was conducted to detect (001) Bragg diffraction peak from intact layered clay platelets. For Cloisite 15A, the (001) plane diffraction was observed at 3.6 nm (q = 1.75 nm^{-1}). In the absence of AC field, the clay platelets were randomly dispersed in blends as indicated by isotropy in diffraction pattern (Fig. 9a-1 and a-2). However, two strong 2D arcs were observed the presence of AC field when X-ray beam was directed orthogonal to the applied electric field direction (Fig. 9a-3 and a-4). Notably, the X-ray scattering pattern was barely changed even after annealing for 120 min. The plot of X-ray intensity as a function of azimuthal angle (ϕ) is shown in Fig. 9b. The similar shape of plots shows that the array of clay platelets were well maintained while PS and PVME polymers undergo phase separation. The orientation of clay platelets for each annealing step with 1000 V/mm AC electric field is shown in Fig. 10a. The clay orientation order parameter was calculated by using the aforementioned procedure (Maier-Saupe distribution function). The clay orientation order parameters was 0.42 before annealing process and then it slightly decreased to 0.4 for 30 min annealing. As annealing time increased, it decreased down to 0.39. This indicates that the oriented clay structure was slightly disordered during phase separation process.

To study the effect of the electric field strength on clay orientation, we investigated the orientation order parameter of clay platelets at various electric field strengths with 60 min annealing samples (Fig. 10b). There was no significant orientation of clay platelets at low field strength (below 100 V/mm), indicating that the clay orientation remained randomized at high annealing temperature. However, the orientation of clay platelets appeared at 200 V/mm with 0.3 orientation order parameter. It increased to 0.35 at 500 V/mm and then it was saturated to 0.37 above 750 V/mm. 2D WAXS technique only presents the orientation factors of large particles (i.e. intact layered clay platelets), not the fully exfoliated clay platelets as they do not form full 3D crystal lattice and not show (001) planes. Hence, the effect of fully exfoliated clay platelets to anisotropic PS / PVME phase-separated morphology domains cannot be addressed by using 2D WAXS technique. Nevertheless, the phase-separated morphology of PS / PVME blends is related to the orientation of the layered clay platelets. The orientation order parameter of domains (Fig. 8f) and that of clay platelets (Fig. 10b) were plotted as shown in Fig. 10c. The results show the linear correlation between orientation of clay and that of polymer domains, showing the slope of this plot is approximately 2. This correlation implies that the degree of orientation of clay platelets influence the anisotropic morphology of PS / PVME blends.

To assess the detailed local morphology of a phase-separated sample, the cross-sectional cryo-microtomed sample was observed by TEM. For the sample annealed at 128 °C for 15 min with 500V/mm, the discrete PS domains in a continuous PVME domain was observed (Fig. 11). The ellipsoidal PS domains in Fig. 11a indicated that PS domains were coarsened and elongated parallel to AC electric field direction. The location and orientation of clay platelets were clearly observed in a magnified image shown in Fig. 11b. Anisotropic clay particles in size from submicron to several microns were observed in a PVME phase by surrounding a discrete PS domain. Most of anisotropic clay platelets were oriented to AC field direction even though some of clay platelets formed several micrometer-sized aggregates. The image of clay particles wrapped around an

ellipsoidal PS domain illustrates how the anisotropic phase separation emerged. The clay particles were initially highly oriented to AC field before phase separation. At the early stage of the phase separation, the co-continuous PS/PVME morphology appeared. Due to the preferential wetting of clay platelets by a PVME component, pre-oriented clay platelets remain in PVME phase in ensuing coarsening process. Furthermore, the coarsening PS domains during the phase separation pushed away the clays so that they appeared to wrap around the PS domains. This mechanism causes the loss of the clay orientation as phase separation continues as evidenced by the time evolution of orientation of clay particles shown in Fig. 9a where the clay orientation slightly decreases as the phase separation takes place. Then, the ongoing anisotropic diffusion of PS domains formed highly directionally organized morphology in the late stage of phase separation.

Lastly, Fig. 12 summarizes the two schematic illustrations of phase-separating morphology with non-oriented and electric field pre-oriented clay platelets. The co-continuous structures emerge in both sample in the early stage of phase separation, indicating that the morphology in this stage was not notably affected by clay pre-orientation. As annealing time elapses, the effect of orientation of clay platelets on the morphology in blends become noticeable as they act as anisotropic barriers to polymer diffusion to ultimately form phase-separated highly directional structures.

Conclusion

We demonstrated that the phase-separated morphology of a PS / PVME polymer blend can be controlled by electrical pre-orientation of organically-modified clay platelets in one phase followed by temperature jump to two phase regime. The isotropic co-continuous morphology undergoing spinodal decomposition in the early stage was followed by coarsening with primary direction of the clay orientation during phase separation. The formation of the anisotropic phase-separated morphology was attributed to preferential localization of pre-oriented clay platelets in PVME domains that affects directionality of diffusion process. This method promises to be a general technique to produce anisotropic polymer films with unique anisotropic electrical, ionic and optical properties.

Conflicts of interest

There are no conflicts of interest to declare.

Acknowledgements

Partial support for this work was provided by NSF (# 1511896) for which the authors are grateful.

References

1 F. S. Bates, *Science*, 1991, **251**, 898–905.
2 C. H. Arns, M. A. Knackstedt, A. P. Roberts and V. W. Pinczewski, *Macromolecules*, 1999, **32**, 5964–5966.
3 J. V. Gasa, R. A. Weiss and M. T. Shaw, *J. Memb. Sci.*, 2008, **320**, 215–223.
4 B. Ray and M. A. Alam, *Sol. Energy Mater. Sol. Cells*, 2012, **99**, 204–212.
5 C. C. Han, Y. Yao, R. Zhang and E. K. Hobbie, *Polymer*, 2006, **47**, 3271–3286.
6 L. Kielhorn, R. H. Colby and C. C. Han, *Macromolecules*, 2000, **33**, 2486–2496.
7 G. Venugopal and S. Krause, *Macromolecules*, 1992, **25**, 4626–4634.
8 G. Venugopal, S. Krause and G. E. Wnek, *Chem. Mater.*, 1992, **4**, 1334–1343.
9 J. M. Serpico, G. E. Wnek, S. Krause, T. W. Smith, D. J. Luca and A. Van Laeken, *Macromolecules*, 1991, **24**, 6879–6881.
10 H. Hori, O. Urakawa, O. Yano and Q. Tran-Cong-Miyata, *Macromolecules*, 2007, **40**, 389–394.
11 M. Gopinadhan, P. W. Majewski, E. S. Beach and C. O. Osuji, *ACS Macro Lett.*, 2012, **1**, 184–189.
12 P. Dommersnes, Z. Rozynek, A. Mikkelsen, R. Castberg, K. Kjerstad, K. Hersvik and J. Otto Fossum, *Nat. Commun.*, 2013, **4**, 2066.
13 G. Taylor, *Proc. R. Soc. A Math. Phys. Eng. Sci.*, 1966, **291**, 159–166.
14 I. Hopkinson and M. Myatt, *Macromolecules*, 2002, **35**, 5153–5160.
15 L. Li, X. Shen, S. W. Hong, R. C. Hayward and T. P. Russell, *Angew. Chem., Int. Ed.*, 2012, **51**, 4089–4094.
16 T. Kwon, T. Kim, F. B. Ali, D. J. Kang, M. Yoo, J. Bang, W. Lee and B. J. Kim, *Macromolecules*, 2011, **44**, 9852–9862.
17 C. Huang, J. Gao, W. Yu and C. Zhou, *Macromolecules*, 2012, **45**, 8420–8429.
18 L. Li, C. Miesch, P. K. Sudeep, A. C. Balazs, T. Emrick, T. P. Russell and R. C. Hayward, *Nano Lett.*, 2011, **11**, 1997–2003.
19 H. J. Chung, K. Ohno, T. Fukuda and R. J. Composto, *Nano Lett.*, 2005, **5**, 1878–1882.
20 S. Gam, A. Corlu, H.-J. Chung, K. Ohno, M. J. A. Hore and R. J. Composto, *Soft Matter*, 2011, **7**, 7262–7268.
21 M. A. Hillmyer, W. W. Maurer, T. P. Lodge, F. S. Bates and K. Almdal, *J. Phys. Chem. B*, 1999, **103**, 4814–4824.
22 J. A. Galloway, H. K. Jeon, J. R. Bell and C. W. Macosko, *Polymer*, 2005, **46**, 183–191.
23 S. P. Lyu, T. D. Jones, F. S. Bates and C. W. Macosko, *Macromolecules*, 2002, **35**, 7845–7855.
24 Y. Wang, Q. Zhang and Q. Fu, *Macromol. Rapid Commun.*, 2003, **24**, 231–235.
25 B. B. Khatua, D. J. Lee, H. Y. Kim and J. K. Kim, *Macromolecules*, 2004, **37**, 2454–2459.
26 M. Si, T. Araki, H. Ade, a. L. D. Kilcoyne, J. C. Sokolov, M. H. Rafailovich and R. Fisher, *Macromolecules*, 2006, **39**, 4793–4801.
27 M. Trifkovic, A. T. Hedegaard, M. Sheikhzadeh, S. Huang and C. W. Macosko, *Macromolecules*, 2015, **48**, 4631–4644.
28 R. Altobelli, M. Salzano de Luna and G. Filippone, *Soft Matter*, 2017, **13**, 6465–6473.
29 K. Yurekli, A. Karim, E. J. Amis and R. Krishnamoorti, *Macromolecules*, 2003, **36**, 7256–7267.
30 L. Bai, J. W. Fruehwirth, X. Cheng and C. W. Macosko, *Soft*

Matter, 2015, **11**, 5282–5293.

31 D. Cai and P. S. Clegg, *Chem. Commun. Chem. Commun*, 2015, **51**, 16984–16987.

32 E. M. Herzig, K. A. White, A. B. Schofield, W. C. K. Poon and P. S. Clegg, *Nat. Mater.*, 2007, **6**, 966–971.

33 S. Batra, E. Unsal and M. Cakmak, *Adv. Funct. Mater.*, 2014, **24**, 7698–7708.

34 H. Koerner, J. D. Jacobs, D. W. Tomlin, J. D. Busbee and R. a. Vaia, *Adv. Mater.*, 2004, **16**, 297–302.

35 D. H. Kim, K. S. Cho, T. Mitsumata, K. H. Ahn and S. J. Lee, *Polymer*, 2006, **47**, 5938–5945.

36 A. Kriisa and C. B. Roth, *J. Chem. Phys.*, 2014, **141**, 134908

37 A. Kriisa and C. B. Roth, *ACS Macro Lett.*, 2019, **8**, 188–192.

38 J. T. Cabral, J. S. Higgins, T. C. B. McLeish, S. Strausser and S. N. Magonov, *Macromolecules*, 2001, **34**, 3748–3756.

39 G. D. Liang and S. C. Tjong, *IEEE Trans. Dielectr. Electr. Insul.*, 2008, **15**, 214–220.

40 K. Pathmanathan and G. P. Johari, *J. Polym. Sci. Part B Polym. Phys.*, 1987, **25**, 379–386.

41 S. Zhang and J. Runt, *J. Phys. Chem. B*, 2004, **108**, 6295–6302.

42 J. K. Yeganeh, F. Goharpey, E. Moghimi, G. Petekidis and R. Foudazi, *Soft Matter*, 2014, **10**, 9270–9280.

43 C. A. Martin, J. K. W. Sandler, A. H. Windle, M. K. Schwarz, W. Bauhofer, K. Schulte and M. S. P. Shaffer, *Polymer*, 2005, **46**, 877–886.

44 H. Behniafar and S. Haghighat, *Polym. Adv. Technol.*, 2008, **19**, 1113–1117.

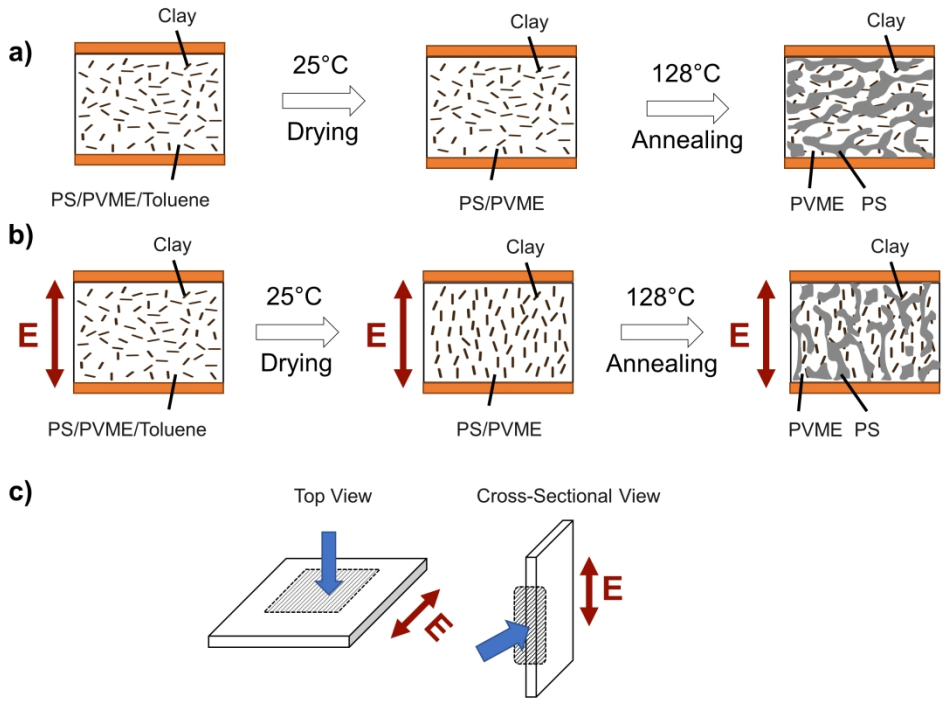

Fig. 1 Schematic illustration of the sample preparation process (a) without electric fields and (b) with electric fields. (c) Direction of top and cross-sectional view of the films for investigating blend morphologies along with AC field direction.

254x177mm (300 x 300 DPI)

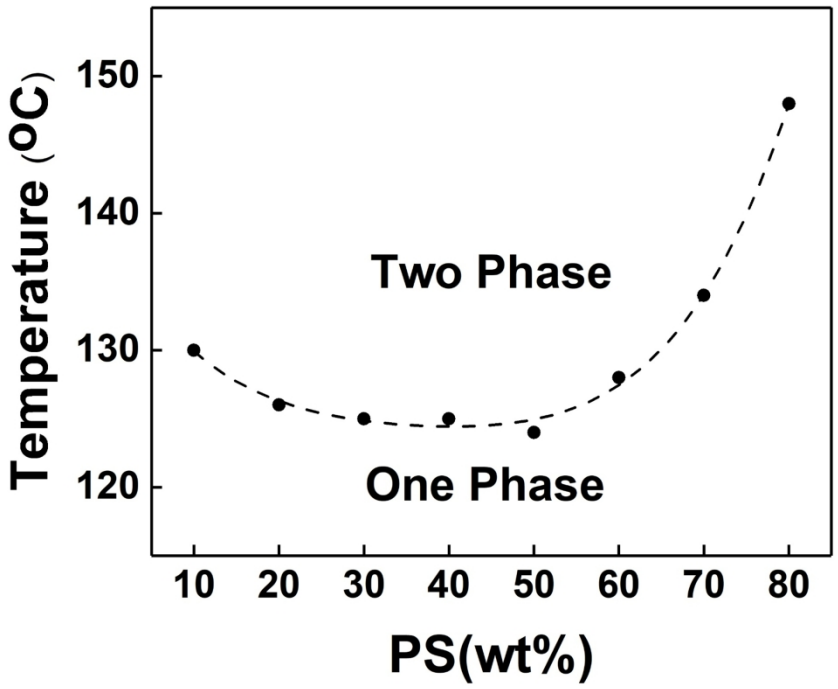

Fig. 2 Phase diagram of a PS / PVME blend. The blend shows a LCST behavior with a critical temperature of 124 °C at 50/50 composition.

254x190mm (300 x 300 DPI)

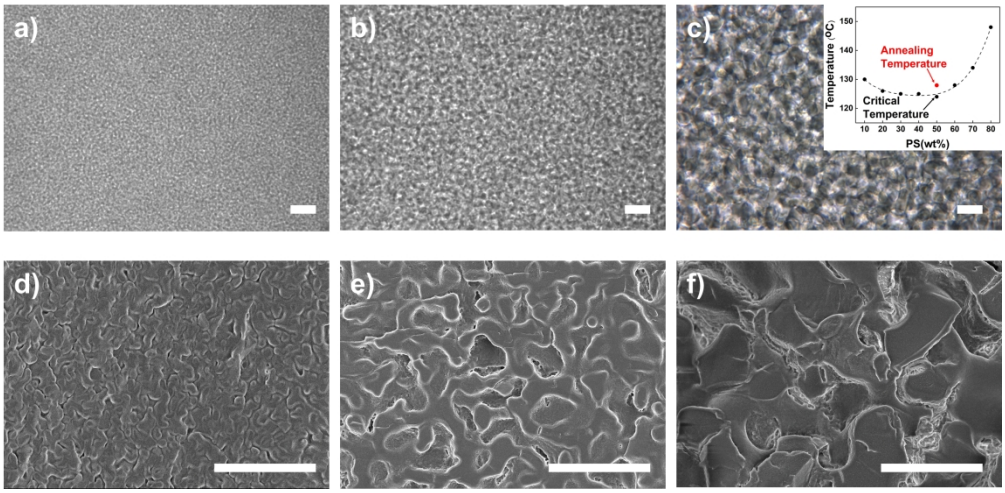

Fig. 3 Phase-separated morphology of a neat PS/PVME (50/50) blend. OM images (Top view, a-c) and SEM images (Cross-sectional view, d-f) annealed for (a, d) 5min (b, e) 7.5 min and (c, f) 10 min at 128°C. (Scale bar: 10μm) (inset: Critical temperature (124°C) and annealing temperature (128°C) are indicated in the Phase diagram of the PS/PVME blend).

250x121mm (300 x 300 DPI)

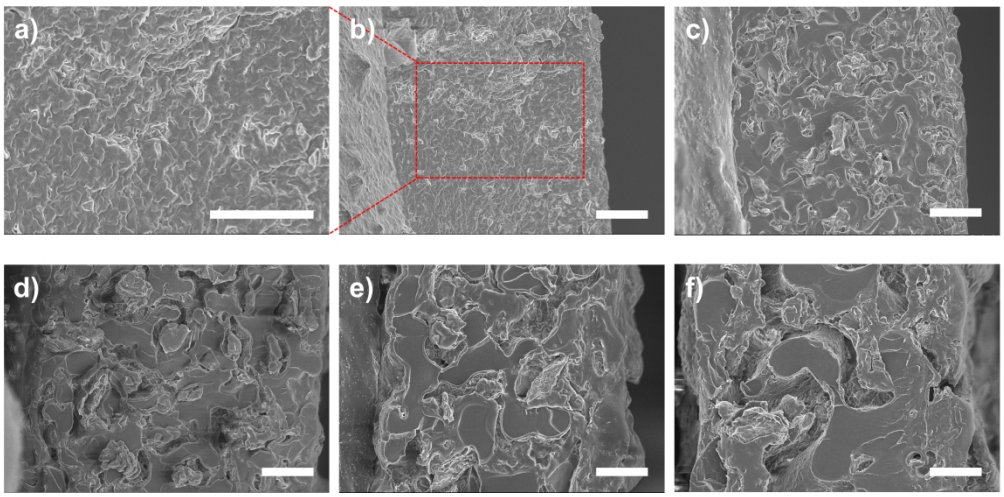

Fig. 4 Cross-sectional SEM images of a PS/PVME (50/50) blend morphology with 5 vol% clay platelets annealed at 128 °C in the absence of AC field. Phase-separated morphology annealed for (a,b) 5min, (c) 7.5 min, (d) 10 min, (e) 12.5 min, and (f) 15min. (Scale bar : 10μm)

250x121mm (300 x 300 DPI)

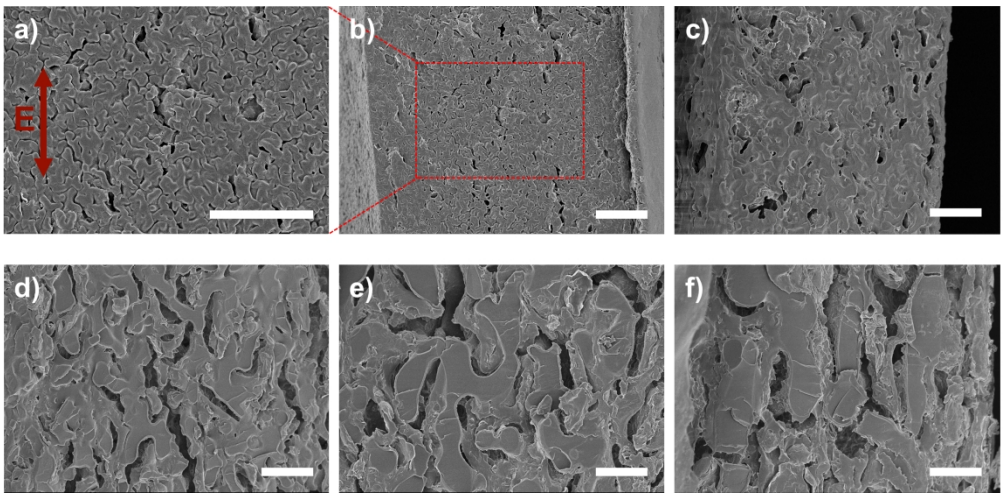

Fig. 5 Cross-sectional SEM images of a PS/PVME (50/50) blend morphology with pre-oriented 5 vol% clay platelets annealed at 128 °C. The arrow indicates the AC field (500V/mm, 100Hz) direction. Phase-separated morphology annealed for (a, b) 5min, (c) 7.5 min, (d) 10 min, (e) 12.5 min, and (f) 15min. (Scale bar : 10μm)

250x121mm (300 x 300 DPI)

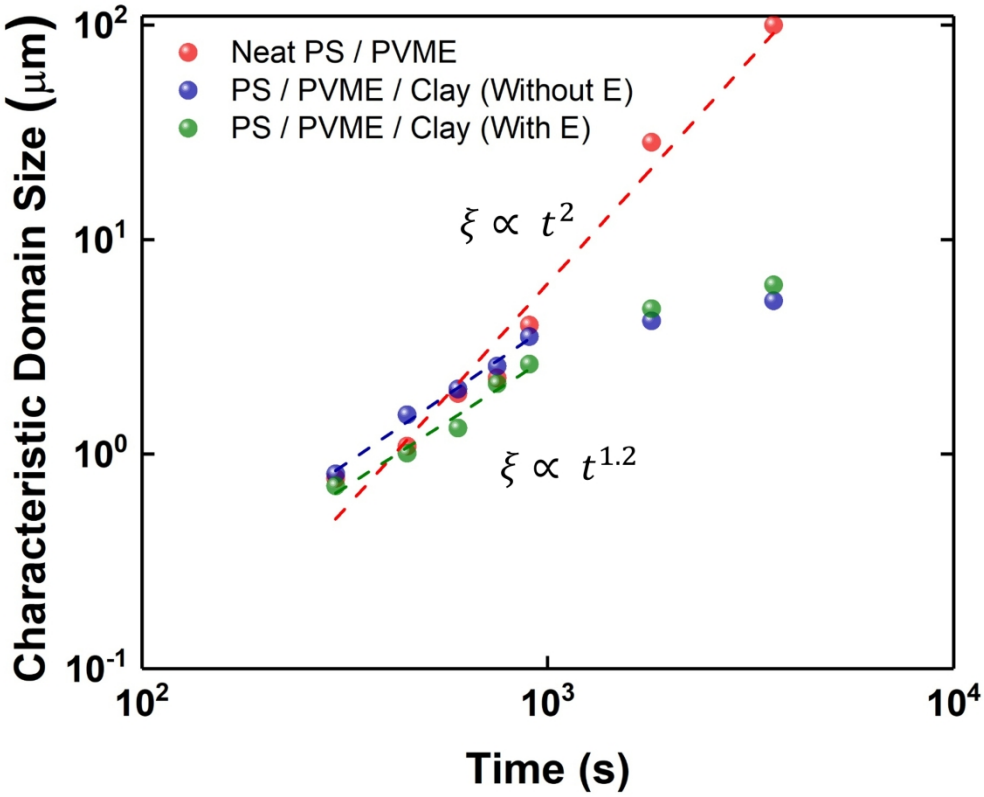

Fig. 6 Characteristic domain size (ξ) over annealing time for PS/PVME (50/50) blends annealed at 128°C. (Red : Neat PS / PVME, Blue: PS / PVME / non-oriented 5 vol% clay platelets, Green : PS / PVME / pre-oriented 5 vol% clay platelets)

215x175mm (300 x 300 DPI)

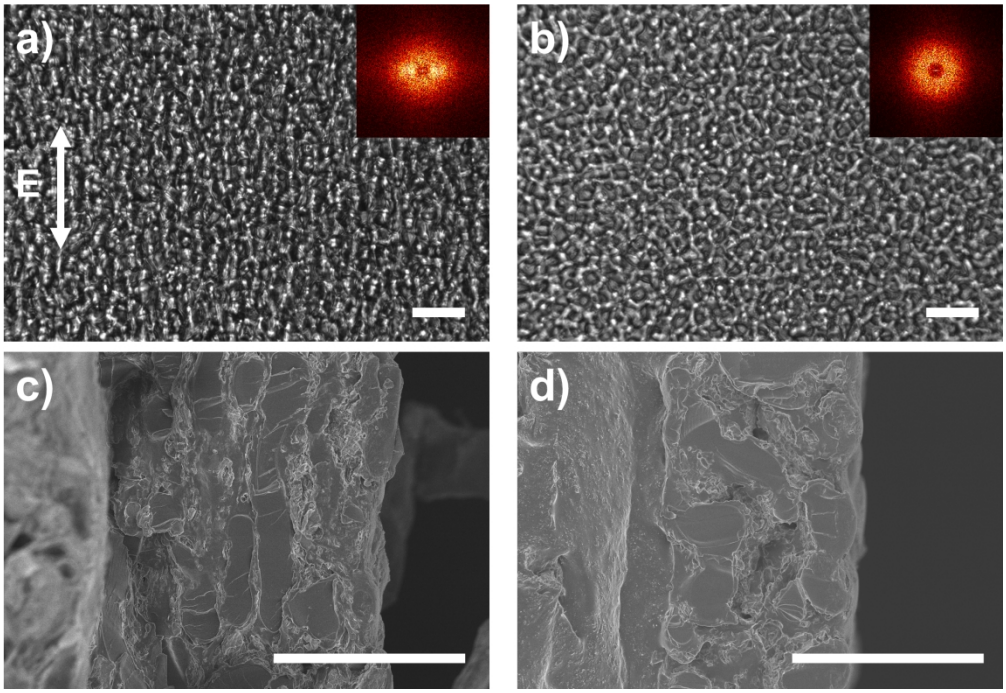

Fig. 7 Phase-separated morphology of a PS/PVME (50/50) blend containing 5 vol% clay platelets annealed at 128 °C for 30 mins with and without the AC electric field. The arrow indicates the AC field (500V/mm, 100Hz) direction. (a) OM images (Top view) and (c) corresponding SEM images (Cross-sectional view) of the sample prepared with AC fields. (b) OM images (Top view) and (d) corresponding SEM images (Cross-sectional view) of the samples prepared without AC fields. (Scale bar: 50μm).

222x152mm (300 x 300 DPI)

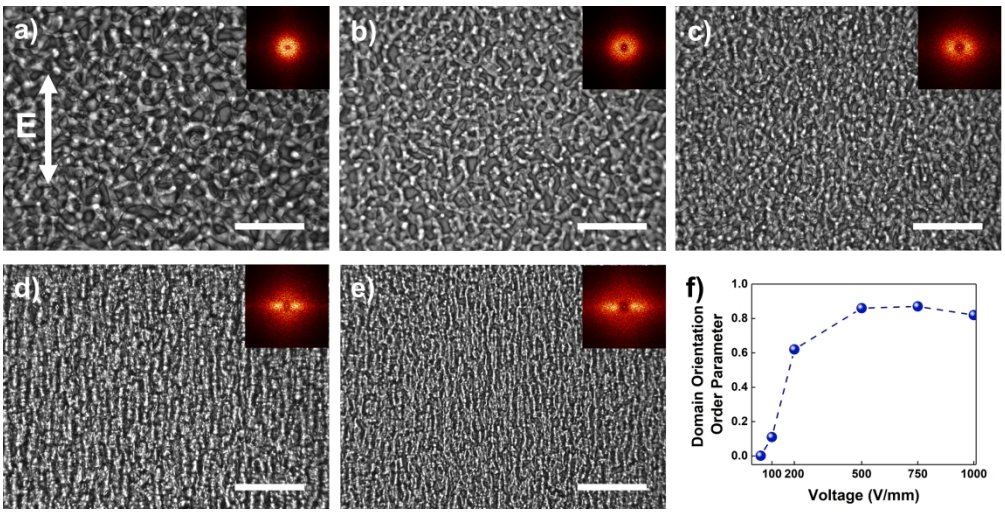

Fig. 8 OM images (Top view) of the PS/PVME (50/50) blend morphology containing 5 vol% clay platelets with various AC electric field strengths for 60 min annealing time at 128 °C. The field strengths are (a) 50V/mm, (b) 100 V/mm, (c) 200 V/mm, (d) 500 V/mm, (e) 1000 V/mm. (f) Plots of the orientation order parameter of polymer domains to various electric field intensity. (Scale bar : 100μm) 2D-FFT patterns of the corresponding OM images are inserted upper right corner.

249x125mm (300 x 300 DPI)

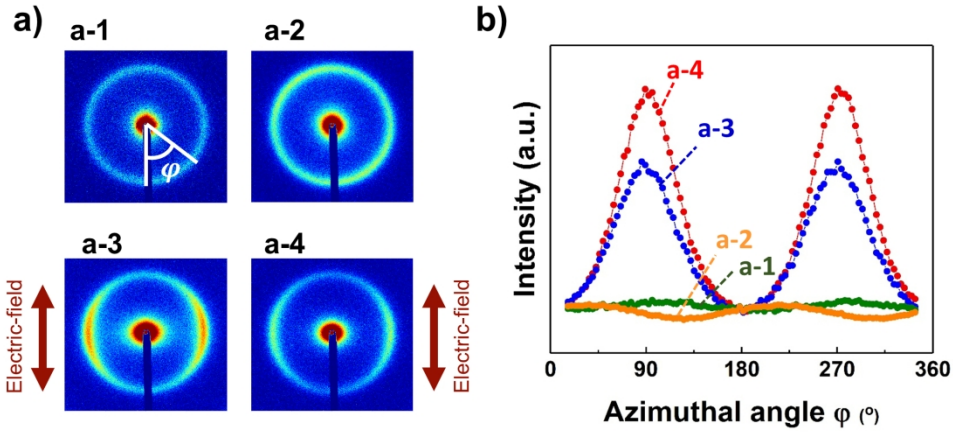

Fig. 9 (a) 2D WAXS scattering pattern of a PS/PVME (50/50) blend containing 5 vol% clay platelets. The sample prepared with (a-1) 0 V/mm and 0 min annealing, (a-2) 0 V/mm and 120 min annealing, (a-3) 1000 V/mm and 0 min annealing, and (a-4) 1000 V/mm and 120 min annealing. (b) The corresponding plot of the integrated intensity of the 2D WAXS pattern against the azimuthal angle.

203x96mm (300 x 300 DPI)

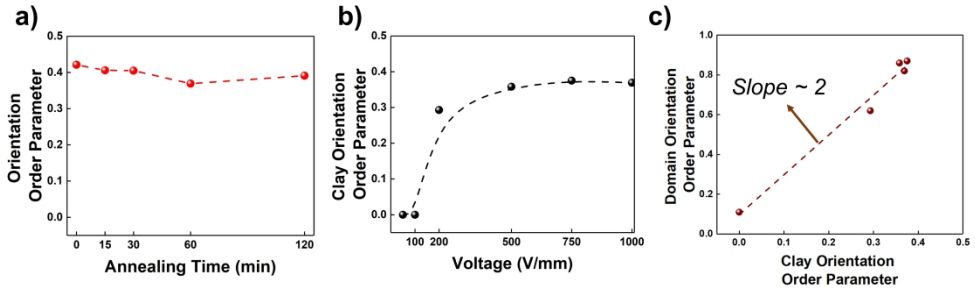

Fig. 10. (a) The orientation order parameter of clay platelets in the samples prepared with the AC electric field (1000 V/mm, 100 Hz) for different annealing times. (b) The orientation order parameter of clay platelets at various electric field strength. (c) The plot of the orientation order parameter of clay to the orientation order parameter of polymer domains.

317x96mm (300 x 300 DPI)

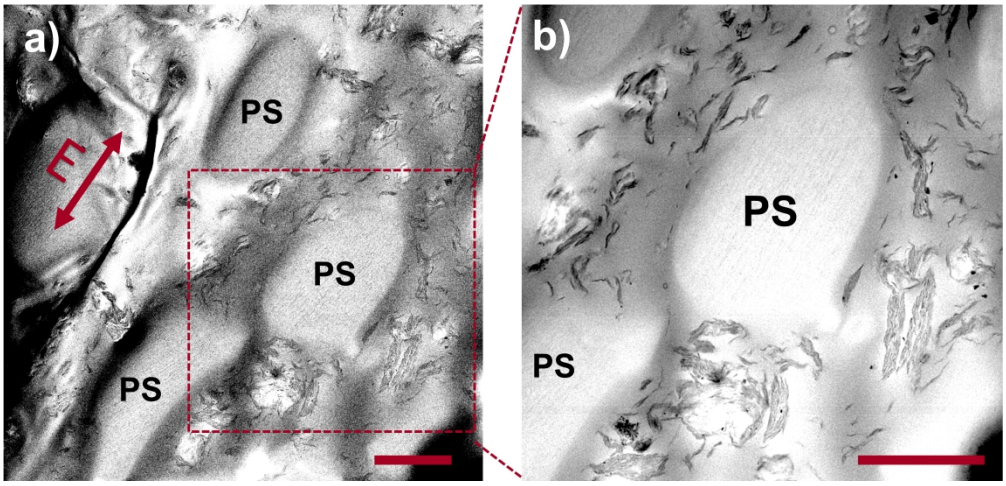

Fig. 11. (a,b) TEM image of the cryo-microtomed sample (PS/PVME (50/50) blend containing 5 vol% clay platelets annealed at 128 °C for 15 min with 500V/mm). (Scale bar: 5 μm)

300x143mm (300 x 300 DPI)

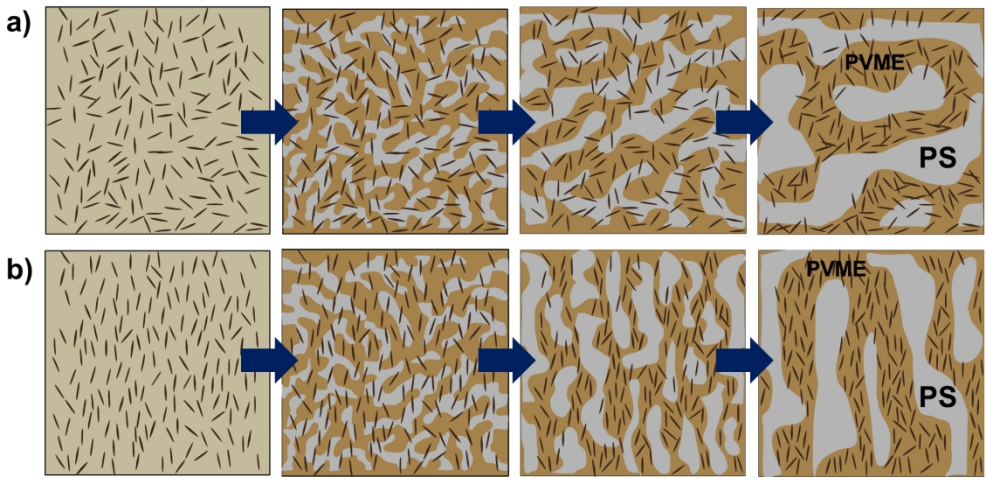

Fig. 12. Cartoons of a PS/PVME phase-separated morphology over annealing time with (a) non-oriented and (b) pre-oriented clay platelets.

195x92mm (300 x 300 DPI)

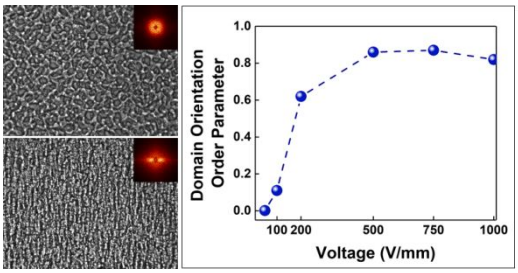

We describe a general pathway to prepare an anisotropic phase-separated blend morphology by using electrically pre-orientated clay platelets.